Dynamic Functional Connectomics Signatures for Characterization and Differentiation of PTSD Patients

Xiang Li,[1] Dajiang Zhu,[1] Xi Jiang,[1] Changfeng Jin,[2] Xin Zhang,[3,1] Lei Guo,[3] Jing Zhang,[4] Xiaoping Hu,[5] Lingjiang Li,[2] and Tianming Liu[1]*

[1]*Department of Computer Science and Bioimaging Research Center, The University of Georgia, Athens, Georgia*
[2]*The Mental Health Institute, The Second Xiangya Hospital, Central South University, Changsha, China*
[3]*School of Automation, Northwestern Polytechnic University, Xian, China*
[4]*Department of Statistics, Yale University, Connecticut*
[5]*Department of Biomedical Engineering, Biomedical Imaging Technology Center, Emory University, Georgia*

Abstract: Functional connectomes (FCs) have been recently shown to be powerful in characterizing brain conditions. However, many previous studies assumed temporal stationarity of FCs, while their temporal dynamics are rarely explored. Here, based on the structural connectomes constructed from diffusion tensor imaging data, FCs are derived from resting-state fMRI (R-fMRI) data and are then temporally divided into quasi-stable segments via a sliding time window approach. After integrating and pooling over a large number of those temporally quasi-stable FC segments from 44 post-traumatic stress disorder (PTSD) patients and 51 healthy controls, common FC (CFC) patterns are derived via effective dictionary learning and sparse coding algorithms. It is found that there are 16 CFC patterns that are reproducible across healthy controls, and interestingly, two additional CFC patterns with altered connectivity patterns [termed signature FC (SFC) here] exist dominantly in PTSD subjects. These two SFC patterns alone can successfully differentiate 80% of PTSD subjects from healthy controls with only 2% false positive. Furthermore, the temporal transition dynamics of CFC patterns in PTSD subjects are substantially different from those in healthy controls. These results have been replicated in separate testing datasets, suggesting that dynamic functional connectomics signatures can effectively characterize and differentiate PTSD patients. *Hum Brain Mapp 00:000–000, 2013.*

Key words: connectivity; diffusion tensor imaging; resting state fMRI

Additional Supporting Information may be found in the online version of this article.

Contract grant sponsor: NIH; Contract grant number: K01 EB 006878NIH R01 HL087923-03S2NIH R01 DA033393NSF CAREER Award IIS-1149260

Contract grant sponsors: University of Georgia start-up research funding; NWPU Foundation for Fundamental Research; The National Natural Science Foundation of China; Contract grant number: 30830046; Contract grant sponsor: The National 973 Program of China; Contract grant number: 2009 CB918303. Contract grant sponsors: Georgia Research Alliance and NIH. Contract grant number: R01 DA033393; Contract grant sponsor: start-up funding and Sesseel Award from Yale University.

*Correspondence to: Tianming Liu, Department of Computer Science and Bioimaging Research Center, The University of Georgia, Athens, GA. E-mail: tianming.liu@gmail.com

Received for publication 2 August 2012; Revised 6 February 2013; Accepted 18 February 2013

DOI: 10.1002/hbm.22290

Published online in Wiley Online Library (wileyonlinelibrary.com).

INTRODUCTION

Connectomes constructed via neuroimaging data offer a complete description of the macroscale structural connectivity within the brain [e.g., Sporns et al., 2005; Van et al., 2010; Hagmann et al., 2010; Williams, 2010; Kennedy, 2010; Zhu et al., 2012b] and functional connectomics signature have been shown to be powerful in characterizing and differentiating brain conditions [e.g., Lynall et al., 2010; Li et al., 2012a]. A typical assumption used in previous functional connectivity and connectomics studies [e.g., Dickerson and Sperling, 2009; Lynall et al., 2010; Li et al., in press] is the temporal stationarity, that is, functional connectivity and functional connectome (FC) are measured over the entire fMRI scan. However, neuroscience research has suggested that the function of the brain is dynamic, and each brain area runs different "programs" according to the context and to the current perceptual requirements [Gilbert and Sigman, 2007]. The dynamically changing functional interactions between structural connections from higher- to lower-order brain areas and intrinsic cortical circuits mediate the moment-by-moment functional switching in the brain [Gilbert and Sigman, 2007]. Therefore, quantitative modeling and characterization of functional brain dynamics has been of general interest in the neuroimaging community for years. For instance, functional microstates have been well-established in EEG data modeling and analysis [Lehmann et al., 1998, 1994, Pascual-Marqui et al., 1995, Koenig et al., 1999, 2002]. Recently, there have been increasing reports on the functional brain dynamics revealed by resting state fMRI (R-fMRI) data. For instance, it has been shown that the brain undergoes dynamical changes of functional connectivity, even in the resting state [e.g., Chang and Glover, 2010; Majeed et al., 2011; Li et al., 2012; Smith et al., 2012; Zhang et al., 2012]. More importantly, quantitative characterization of these time-dependent functional connectivity/connectome dynamics and representative patterns can elucidate fundamentally important temporal attributes of functional connections that cannot be seen by traditional static pairwise functional connectivity analysis [e.g., Smith et al., 2012; Li et al., 2012].

From a technical perspective, the discovery, cross-validation and application of EEG-based microstates have been fundamentally enabled and facilitated by a standardized electrode reference system such as the International 10/20 System [Niedermeyer and Silva, 2004]. As a result, the measured EEG signals and the identified dynamic microstates in different brains can be readily mapped into a standard reference system, and thereby effectively integrated and compared. However, for R-fMRI data, it has been challenging to integrate and compared fMRI signals and their derived measurements across different brains due to the lack of a reliable and accurate brain localization and reference system. Because of the remarkable variability of the structural and functional architecture of the cerebral cortex [e.g., Zilles and Amunts, 2010; Liu, 2011], defining a common and consistent set of cortical landmarks across different brains remains as one of the major barriers in human brain mapping [Derrfuss and Mar, 2009; Poldrack, 2012]. Recently, we have developed and validated a large set of consistent and correspondent cortical landmarks (named Dense Individualized and Common Connectivity-based Cortical Landmarks, or DICCCOL) [Zhu, et al., 2012b], each of which was optimized to possess maximal group-wise consistency of diffusion tensor imaging (DTI)-derived fiber shape patterns [Zhu, et al., 2011, Zhu, et al., 2012a,b]. The neuroscience basis is that each brain's cytoarchitectonic area possesses a unique set of intrinsic inputs and outputs, namely the "connectional fingerprint" [Passingham et al., 2002], which largely determines the functions that each brain area performs. This close relationship between consistent structural connection pattern and brain function has been replicated in a series of our recent studies [Zhu et al., 2011, Zhu et al., 2012a,b; Li et al., 2010, Zhang et al., 2011]. This set of 358 DICCCOL landmarks has been reproduced in over 240 brains of four separate healthy populations [Zhu et al., 2012b]. Importantly, this set of 358 DICCCOL landmarks can be accurately predicted in an individual subject based only on DTI data [Zhu et al., 2011, Zhu et al., 2012a, Zhang et al., 2011]. The collection of 358 DICCCOL landmarks and their prediction source codes are publicly available at: http://dicccol.cs.uga.edu.

As these DICCCOLs possess intrinsically established structural and functional correspondences across individuals, they provide a natural general brain reference system across individuals and populations [Zhu et al., 2012,b]. In addition, it has been shown that functional connectomics signatures derived from the DICCCOL system can effectively characterize and differentiate brain conditions from healthy controls [Li et al., in press]. Therefore, in this article, we used DICCCOL to construct structural and FCs to define and characterize functional microstates based on R-fMRI data with the hypothesis that functional connectomics signatures can effective characterize and differentiate post-traumatic stress disorder (PTSD) patients. In particular, we used the large-scale functional connectivity among DICCCOLs as FC, and divided the temporally varying FCs into quasi-stable segments via the approaches in Zhang et al. [2012] and Li et al. [2012]. For instance, a typical R-fMRI scan with time length of 10 min can be segmented into 10–20 quasi-stable FC segments, within which the FCs are averaged into one vector. Given that the averaged FCs possess intrinsically established correspondences across individuals, all of the averaged FCs from 95 brains are pooled and clustered into 16 common FCs (CFCs) via the Fisher Discriminative Dictionary Learning (FDDL) algorithm [Yang et al., 2011; Zhang et al., 2012]. Our

experimental results showed that these 16 CFC patterns are remarkably reproducible across healthy controls and PTSD patients, and interestingly, two additional CFC patterns with altered connectivity patterns [termed signature FC (SFC)] exist dominantly in PTSD subjects. More importantly, these two SFC patterns alone can successfully differentiate 80% of PTSD subjects from healthy controls with only 2% false positive. These results suggest that SFC patterns could be potentially used as the biomarkers of PTSD in the future.

Furthermore, based on the clustered CFCs, the time series R-fMRI data was projected into a series of temporally concatenated CFCs and their temporal transitions patterns were modeled by a finite state machine (FSM) [Black, 2008]. Essentially, the graph structure and the edge connection strength of the FSM characterize the probability of transition from one CFC pattern to another. Our experimental results revealed that meaningful and reproducible FSMs can be learned from separate groups of brains. In particular, it was found that the FSM learned from PTSD subjects exhibits a substantially altered pattern of CFCs and transition patterns, in comparison with the healthy controls. These results suggest that not only the CFCs patterns themselves but also their temporal transition patterns, can contribute to the characterization and differentiation of PTSD subjects from healthy controls.

In general, the DICCCOL-based universal brain reference system enabled the integration, comparison and cross-validation of the CFCs in R-fMRI data. Otherwise, the functional brain states represented by large-scale FCs in different brains are not readily comparable, and thus cannot be pooled and integrated for group-level or individual level analysis. In this sense, the DICCCOL landmarks are equivalent to the standardized reference electrodes in EEG recordings. With the availability of the well-characterized CFCs as the basic building blocks, the functional status of the brain revealed by R-fMRI data can be decomposed into a series of temporally concatenated CFCs. Essentially, the work in this article has demonstrated that PTSD, as a psychiatric brain condition, can be robustly characterized and differentiated by abnormal CFCs and their altered temporal transition patterns. The remaining three sections will provide details on data acquisition and algorithmic methods, experimental results and their interpretation, as well as discussions and conclusions.

MATERIALS AND METHODS

Data Acquisition and Preprocessing

PTSD patients and healthy controls were recruited after the 2008 Wenchuan earthquake, Sichuan, China, under IRB approvals. Informed consent was obtained from all subjects after explaining or reviewing detailed written information about the study protocol. Adult PTSD subjects who lived in temporary housing after the Wenchuan earthquake were diagnosed based on the Structured Clinical Interview for DSM-IV (SCID-I/P) and the Clinician-Administered PTSD Scale (CAPS) by experienced psychiatrists (co-authors in this article). The exclusion criteria for the PTSD group included any other current psychiatric disorders, any lifetime psychiatric disorders based on SCID or MINI-KID, a history of head trauma or loss of consciousness, any significant medical, neurological conditions, any endocrine disease, taking any anti-psychotic drugs, taking any antidepressant drugs, taking any benzodiazepines 1 month before scan, drinking alcohol 1 week before scan, using any other psychoactive substances such as cocaine or ketamine, pregnancy, and nonright handed. Gender and age (within 2 years), as well as education (within 5 years), matched controls were recruited from temporary houses in the same Wenchuan earthquake area. Matched subjects had been equally exposed to the severity of the earthquake at the same time, but did not have PTSD. They had the same interview as PTSD patients and were subjected to the same exclusion criteria. PTSD and healthy controls participated in brain scans at 9 months to 15 months after the earthquake. They were re-interviewed by SCID or MINI-KID and CAPS or (CAPS-CA) on the day of scanning for confirmation of their diagnosis.

DTI and R-fMRI datasets of 95 adult subjects, including 51 healthy control subjects, and 44 PTSD patients were acquired on a 3T MRI scanner in West China Hospital, Huaxi MR Research Center, Department of Radiology, Chengdu, China, under IRB approvals. Acquisition parameters for the scans were as follows. R-fMRI: 64×64 matrix, 4-mm slice thickness, 220 mm FOV, 30 slices, TR = 2 s, total scan length = 400 s; DTI: 256×256 matrix, 3-mm slice thickness, 240 mm FOV, 50 slices, 15 DWI volumes, b-value = 1000. Preprocessing steps of the multimodal DTI/R-fMRI datasets can be found in our recent publications [Zhu et al., 2012b; Zhang et al., 2011; Li et al., 2012; Zhang et al., 2012].

Construction of Structural Connectomes

In this work, the 358 consistent DICCCOL landmarks that have been discovered and validated in our recent study [Zhu et al., 2012b] are localized in the DTI data of each individual subject, based on the cortical landmark prediction approach described earlier [Zhang et al., 2011; Zhu et al., 2012b]. In short, the prediction utilized the fact that there exists consistency in structural connection patterns across human brain [Zhu et al., 2011, Zhu et al., 2012a], and each DICCCOL is defined by the group-wise consistent white-matter fiber connection patterns derived from DTI data. The prediction process includes three major steps: initial landmarks selection, optimization of landmark locations, and determination of group-wise consistent DICCCOLs [Zhu et al., 2012b], and has been proven to be very consistent and reproducible through replication experiments across over 240 brains [Zhu et al., 2012b]. The

visualizations of 358 DICCCOLs have been released online at: http://dicccol.cs.uga.edu, and an illustration of the predicted DICCCOLs in this dataset is shown in Supporting Information Figure S1. Based on the predicted 358 DICCCOLs in each subject with DTI data, the structural connectomes were constructed via published methods [Zhu et al., 2012b], which provide the structural substrates for the definition of FCs in the next section.

FCs and Temporal Segmentation

As mentioned earlier, the functional brain connectivity undergoes temporal dynamic changes even in resting state [e.g., Chang and Glover, 2010; Majeed et al., 2011; Li et al., 2012; Smith et al., 2012; Zhang et al., 2012]. Therefore, we applied a sliding time window approach [Li et al., 2012; Zhang et al., 2012] to divide the extracted R-fMRI signal X_i from the ith DICCCOL into temporal segments $\mathrm{TF}_{i,t}$ at time point t, with the duration of window length l:

$$\mathrm{TF}_{i,t} = \{X_{i,p} | t \le p < t + l\} \quad (1)$$

where $X_{i,\mathrm{p}}$ is the value of time series X_i at time point p. In this work, the sliding time window length l was determined experimentally. In the experiments, we tried the length range of 10–50, in which the range of 10–20 would not change the result significantly. We empirically used the length of 14 that achieved stable and relatively good classification result. For every pair of temporal segments $\mathrm{TF}_{i,t}$ and $\mathrm{TF}_{j,t}$ of the time series X_i and X_j from two DICCCOLs, we calculated the Pearson correlation $R_{i,j,t}$ between them:

$$R_{i,j,t} = \mathrm{corr}(\mathrm{TF}_{i,t}, \mathrm{TF}_{j,t}), \quad R_{i,j,t} = 0, \quad \text{if } i = j;$$
$$\mathrm{FC}_t = \{R_{i,j,t} | i, j \in (1, 358)\} \quad (2)(2)$$

where FC_t is the FC at time t, which is a set of correlations from the congregation of all $R_{i,j,t}$ over every combination of i and j, to characterize the whole-brain functional connectivity. It is a 358×358 symmetric matrix. For visualization and dimension reduction, we defined the FC strength (FCS) as:

$$\mathrm{FCS}_t \sum_{j=1}^{358} R_{i,j,t}, \ \mathrm{FCS} = \{\mathrm{FCS}_1, \mathrm{FCS}_2, \ldots, \mathrm{FCS}_{T-l}\} \quad (3)$$

where FCS_t is the summation of correlations of each DICCCOL region of interest (ROI) with all the other ROIs at time t, which is an $I \times 1$ vector. Thus, the ith value in the vector is the strength of connectivity of the ith ROI. FCS is the aggregation of FCS_t, representing the dynamics of connectome strength through the entire time course. An example of calculating FCS for a randomly selected subject is illustrated in Figure 1. It can be clearly observed from Figure 1 that FCS has clear state-like dynamics pattern, for example, functional connectivity undergoes abrupt changes, although the FCS remains quasi-constant during certain length of time. For visualization purpose, each quasi-stable time period is marked by blue lines as a FC segment in Figure 1. Such temporal pattern has been replicated in all of the 95 cases with R-fMRI datasets. The temporal FC segments of each subject are manually divided, by two expert observers, into quasi-static brain states. Each state is defined as a time period (t_1, t_2) during which functional connectivity across DICCCOLs remains quasi-stable. The criteria used here for definition of quasi-static brain states are similar to those in Zhang et al. [2012] and Li et al. [2012]. The total number of interactively segmented FCs in each subject is approximately with the range of 15–25, and the detailed statistics of the interactive FC segmentation are provided in Table I.

Based on the abovementioned interactive segmentation result of FCs, the dynamics of FCs can be described by the characteristics of brain states as:

$$\mathrm{FCS}_{\mathrm{state_i}} = \sum_{n=t_1}^{t_2} \mathrm{FCS}_t / (t_1 - t_2), \ \text{Where State}_\mathrm{i} = \{t_1, t_1 + 1, \ldots t_2\} \quad (4)$$

where FCS of each brain state $\mathrm{FCS}_{\mathrm{state}}$ is defined as the averaged FCS of temporal segments within this state bounded by (t_1, t_2). In this work, the R-fMRI data of 95 brains (44 PTSD patients and 51 healthy controls) were divided into 2,044 temporally quasi-stable states, in which PTSD patient group has 1,137 segments and healthy control group has 907 segments.

CFC Modeling

In recent years, it has been widely reported that sparse coding methods exhibit very good performance in image analysis, especially in signal and image classification [e.g., Wright et al., 2009; Zhang and Li, 2010; Ramirez et al., 2010]. In this work, the recently developed Fisher Discrimination Dictionary Learning (FDDL) algorithm [Yang et al., 2011] based on Fisher discrimination criterion [Duda et al., 2000] was used to identify CFCs in R-fMRI data. The basic idea of FDDL is to learn a structured dictionary D from the training data A so that $A = DX$, where X is the coding coefficient. D contains certain numbers of sub-dictionary D_i that corresponds to the class labels in the training data, under the constraint of maximizing the discriminative capacity of the dictionary. We first applied the K-means clustering method on A to obtain labels on the data, that is, each training sample was assigned an index. Then, the Bayesian Information Criterion (BIC) [Schwarz, 1978] was used to identify the optimal number of classes (i.e., model

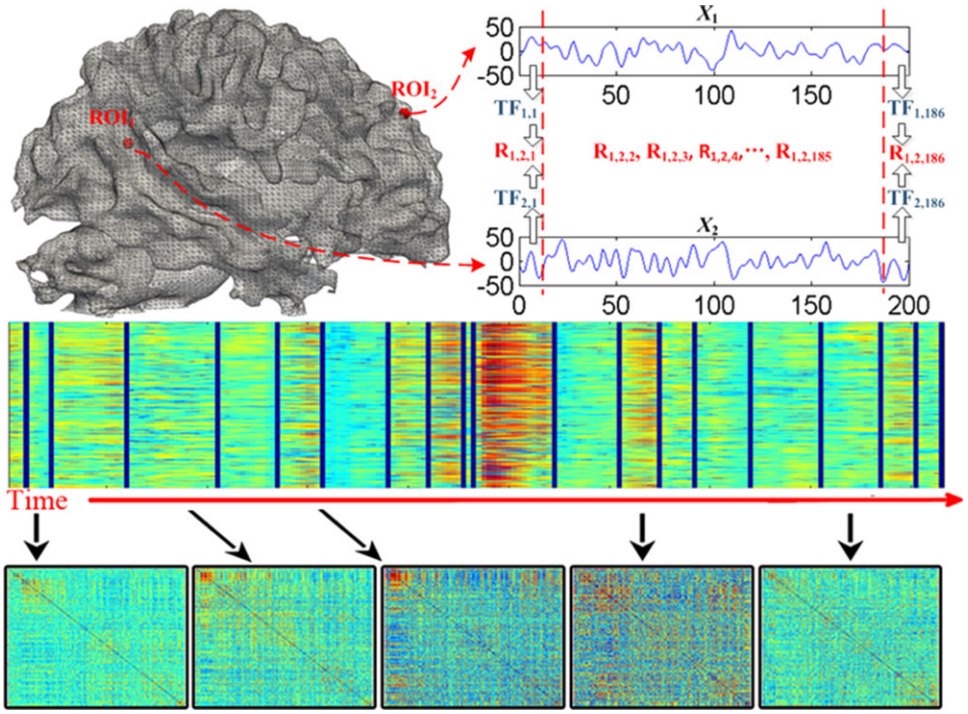

Figure 1.

Illustration of calculating FC and FCS. Top panel: Illustration of R-fMRI signals extracted from two DICCCOL ROIs of a randomly selected subject, X_1 and X_2, and their sliding time-windowed functional correlation $R_{1,2,1}$ to $R_{1,2,186}$; Middle panel: FC strength (FCS). Each column is a single FCS_t at one window, and each row is the dynamics of the connectivity strength of one DICCCOL ROI. The connectome strength is normalized to 0–1, and is color-coded by the level of strength. The dark blue lines highlight manual segmentation results, which are abrupt change points between functional states. Bottom panel: Several averaged FCs of segmented states, which are color-coded matrices, with arrows pointing to their corresponding time periods in the FCS.

order) for the dictionary learning. The criterion is defined as:

$$\mathrm{BIC} = n\,\mathrm{In}\left(\hat{\sigma}_e^2\right) + k\mathrm{In}(n) \tag{5}$$

where σ_e^2 is the estimation for error variance, and in this study it is defined as the summed variance of each state within its corresponding class, n is the total number of states in training matrix A, and k is the number of classes. A larger σ_e^2 indicates that the brain states are more scattered within each class, which is contrary to our goal in dictionary learning. When n is equal to 1, the σ_e^2 would reach its maximum, which is equal to the variance of the original data without any classification. Conversely, a larger n means we are using more classes in the dictionary to reconstruct the data, which is also against our goal. When n is equal to the number of states, σ_e^2 would reach its minimum 0 as each state is within a single class by itself. The trade-off between the model order and the error variance is balanced by the BIC value, and the optimized number of states is determined by finding n to minimize

TABLE I. Summary for interactively segmented FCs including the average numbers, durations, and the statistics for relatively long and short segments (measured by time points)

	Average number	Average duration of states (slices)	Number of states with duration > 15 with duration <5	Number of states with duration < 5	% of states with duration > 15
Healthy Control	17.78	10.46	1.24	4.47	8.39%
PTSD Patients	24.84	7.2	0.78	7.66	3.38%

All the numbers listed are per subject, for example, there are 17.78 interactively segmented FCs per subject on average.

BIC value from the experimental result through searching a range of model orders.

Then, the following energy function $J(D,X)$ were optimized to obtain the learned dictionary D and its corresponding projection X of the data on D [Yang et al., 2011]:

$$J_{(D,X)} = \text{argmin}_{(D,X)}\{r(A,D,X) + \lambda_1 X_1 + \lambda_2 f(X)\} \quad (6)$$

$$r(A,D,X) = A_m - DX_{mF}^2 + A_m - D_m X_{mF}^{m2} + \sum_m^c D_m X_{mF}^{m2} \quad (7)$$

$$f(X) = tr(\sum_{m=1}^{c}\sum_{x_k \in X_m}(x_k - \overline{X_m})(x_k - \overline{X_m})^T - tr\sum_{m=1}^{c} n_m(\overline{x_m} - \overline{X})(\overline{x_m} - \overline{X})^T) + \eta X_F^2 \quad (8)$$

The first term in the energy function, $r(A, D, X)$, is the constraint on discriminative fidelity, allowing the dictionary D able to code the data A (which is the congregated FCS_{states} matrix) with minimum residual, while at the same time only using one subdictionary D_m, but not other subdictionaries. The neuroscience rationale behind it is that each subdictionary D_m learned is corresponded to one way of the classification of FCS_{state}, where within this class the FCS_{state} are similar with each other, and X is the projection of the dataset A on dictionary D, thus it is the classification result (class labels). In Eq. (7), X_m is the projection of A_m, which is one of the subclasses in A, on the whole dictionary D. X_m^m is the projection of A_m on the correct subdictionary D_m. X_m^m is the projection of A_m on other incorrect subdictionaries other than D_i. Thus, to minimize Eq. (7), we requires the optimized dictionary and its corresponding classification to use the correct subdictionary D_m to project A_m, and avoid using other subdictionaries.

The second term in the energy function in Eq. (6) is the sparse constraint, requiring the coding coefficient X be as sparse as possible, that is, the total number of nonzero items in X should be minimized. With this constraint, each single FCS_{state} in A would only be projected by a limited number of subdictionaries, which is in accordance with our premise that the brain states would be discrete with abrupt change on the boundaries. The third term $f(X)$ is the constraint on the discriminative coefficient, which aims to minimize within-class scatter of X, and maximize cross-class scatter of X, according to Fisher discrimination criterion [Duda et al., 2000]. In the definition of $f(X)$, X_k is the item (single FCS_{state}) in X_m, that is, each class of the projection. The within-class scatter of the projection was measured by the summed distance from each item in the class (x_k) to the average of the class ($\overline{X_m}$). The cross-class scatter was measured by the summed distance from the average of each class ($\overline{X_m}$) to the average of the whole data ($\overline{X}$). The integer c is the total number of classes in the training data A, as well as the total number of subdictionaries in dictionary D. The integer n_i is the number of items in X_i, as there are multiple items in each class of the training data A, and η is the scaling constant.

In the energy function, there are three parameters scaling the trade-off between three terms: value of 1 (discriminative fidelity constraint), λ_1 (sparseness constraint), and λ_2 (discriminative scatter constraint). We estimated these parameters based on the premise that there would be substantial alteration of the functional connectivity in the PTSD patients, which has been previously reported [Fonzo et al., 2010; Lanius et al., 2010; Hughes and Shin, 2011]. Thus the optimization would be aimed at maximizing the capacity of the model in discriminating the healthy control subjects from the PTSD subjects in the training data based on their functional connectivity patterns, that is, CFCs. By trying the parameter combination within the range predetermined by the scale of the three terms, we selected the value of parameter λ_1 (0.01) and λ_2 (0.05) so that the model could obtain maximum difference in the distribution of CFCs between healthy control and PTSD subjects. To verify that the parameters estimated from the training dataset are optimal, we applied the models with different parameter combinations on the testing data in a similar fashion. It was found that the same value of parameters ($\lambda_1 = 0.01$, $\lambda_2 = 0.05$) had been estimated on the testing dataset, suggesting that the parameter selection method used in this work is valid and stable.

The learned dictionary has the same dimension with the input training matrix A, and contains subdictionaries corresponding to each class label. Also, as every state has its own FC depicted in Figure 1, we obtained the average FC for each subdictionary, defined as CFC in our study. The dynamics of brain connectomes could then be projected into the small number of representative CFCs with minimum information loss. The learned dictionary was then applied to classify the testing matrix T, to project brain state in testing data to the CFCs. The sparse coding algorithm is based on the sparseness function developed in (Olshausen and Field, 1996) and further enhanced in [Wright et al., 2009] as:

$$\hat{X} = \text{argmin}_{(X)} X_1, \text{subject to } T = \text{DX} \quad (9)$$

where D is the dictionary learned from training samples and T is the testing data. The projection resulted in a vector with the length of total number of states; each value in the vector is the labeling result (an integer) of the corresponding testing sample. An example of the projection result is shown in Supporting Information Figure S2.

RESULTS

Sixteen CFCs Inferred from R-fMRI Data of Healthy Controls

As described in "FCs and Temporal Segmentation" Section, there were 907 brain states manually segmented from 51 healthy control subjects, and each state could be characterized by its corresponding 358*1 FCS_{state} vector. Since

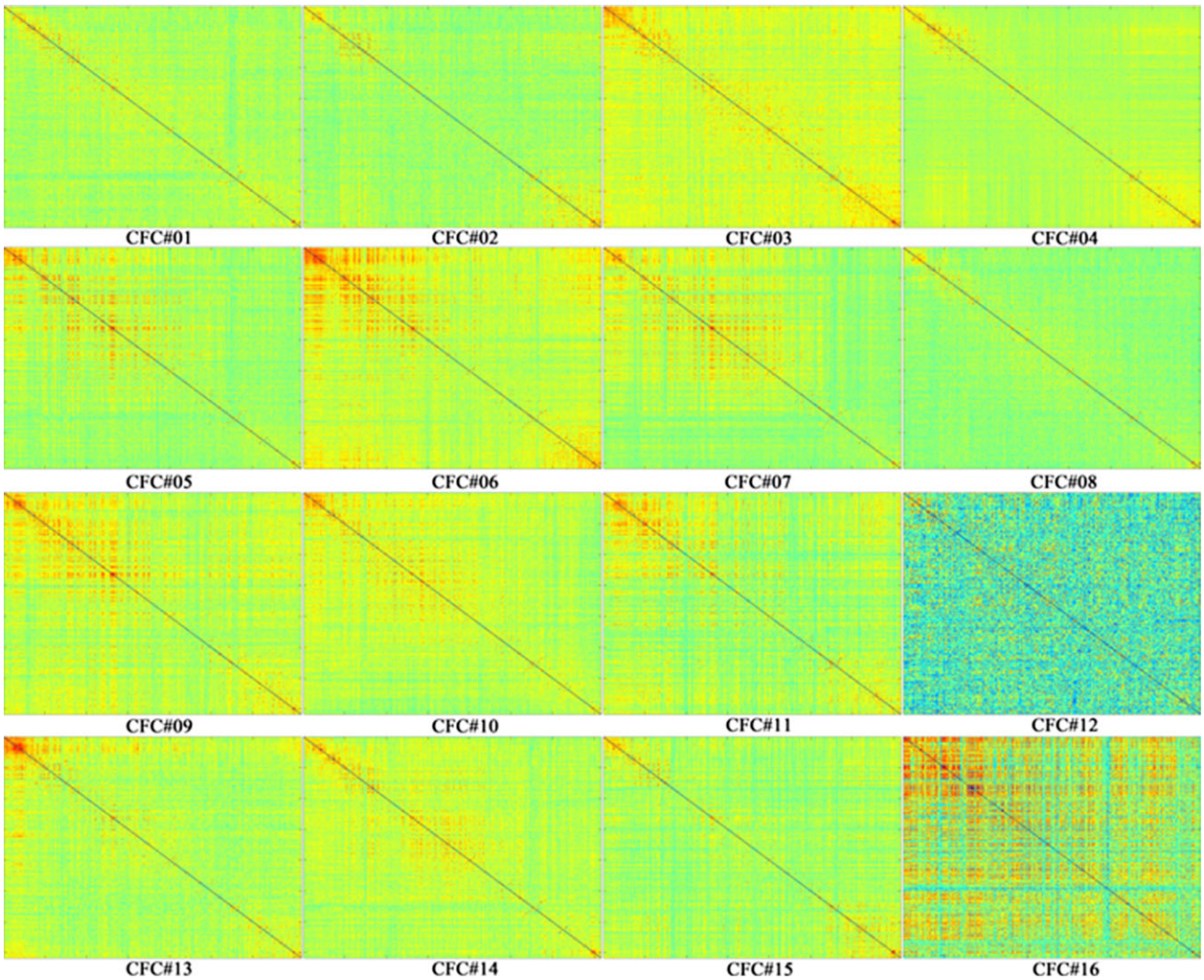

Figure 2.

Visualization of 358 $\times$ 358 connectivity patterns of 16 CFCs obtained by the dictionary learning from healthy controls. Matrices are color-coded according to the strength of functional interaction between the ROI labeled by the column index, to the ROI labeled by the row index. CFCs are ordered by their corresponding frequency of occurrence in the projected temporal segments of all subjects.

the DICCCOL definition of ROIs provided us an inherently universal coordinate system across all the subjects, we could congregate all the FCS_{state} together into a 907×358 matrix, which is the characterization of group-wise functional connectivity strength of healthy control subjects. Then the FDDL model was applied to the congregated data to identify the common functional connectivity patterns across subjects.

The total number of classes for dictionary learning, which was also the number of CFCs, was optimally determined as 16 by the BIC criteria (details in Supporting Information Fig. S3). Based on the estimation of model order, 16 CFCs were identified from brain functional connectivity strength of healthy controls, as shown in Figure 2. The patterns of these 16 CFCs are visualized on the cortical surfaces in Figure 3. Based on the results in Figures 2 and 3, it can be easily appreciated that the brain exhibits remarkably different FC patterns even in resting state, in agreement with prior reports on the functional dynamics of the brain, for example, Chang and Glover [2010], Majeed et al. [2011], Smith et al. [2012], Li et al. [2012]. The novel contribution of the present work is that we quantitatively characterized the representative CFCs of the whole FCs at the population level. The neuroscience meanings of these 16 CFCs are interpreted as follows. The most frequent CFCs (#1–#2) involve strong activities in the default

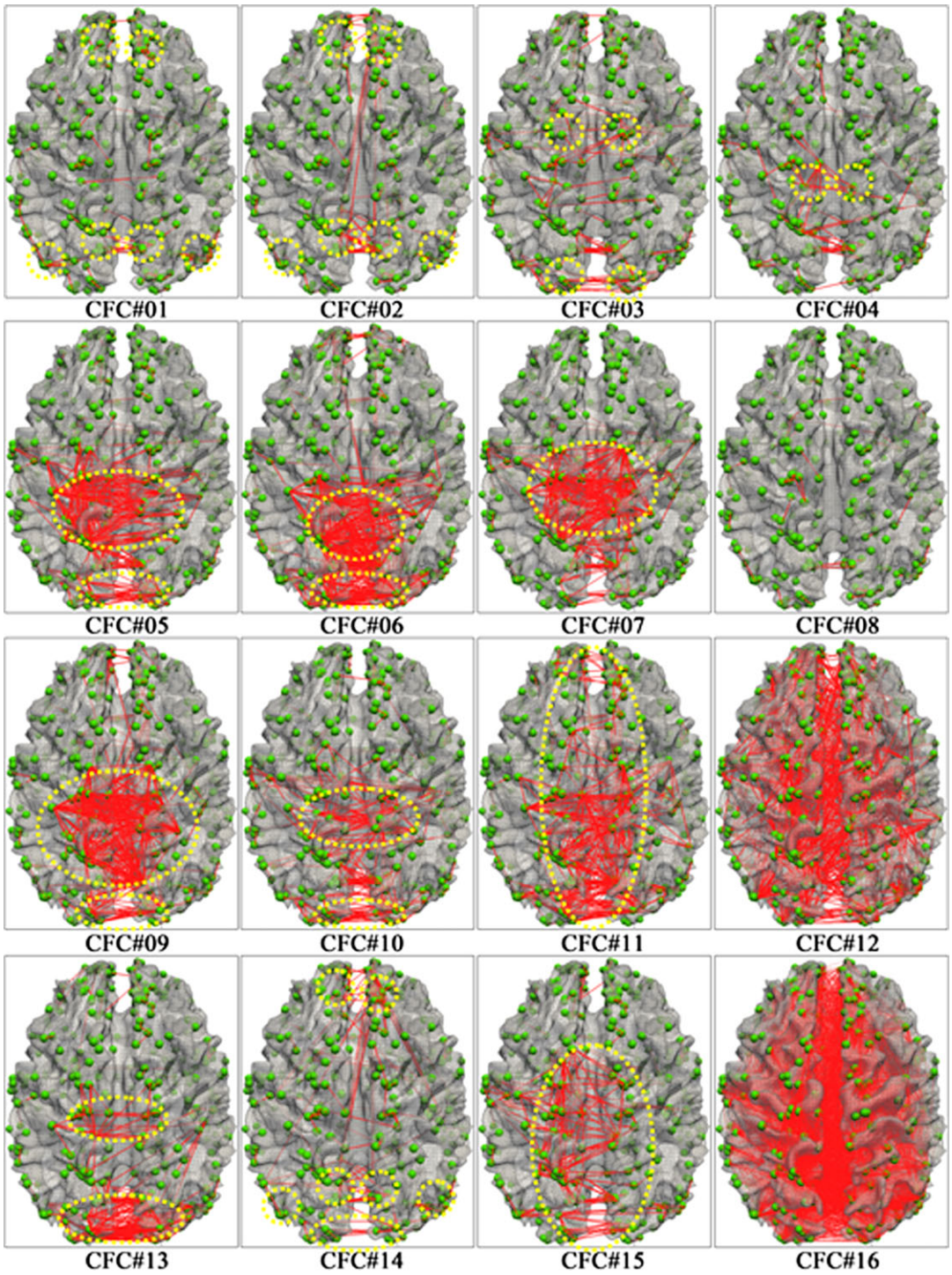

Figure 3.

Visualization of CFCs on cortical surfaces. DICCCOL ROIs are marked as green spheres on the cortical surface, and the functional connectivities between ROIs are shown as red edges connecting those spheres. A threshold (threshold = 0.75 for Pearson's correlation) was used to select the highest functional connectivities that are shown here. The yellow circles in the first row highlight the nodes involved in the DMN.

TABLE II. List of relative difference of CFCs distribution from the training and testing datasets

Fold#01	Fold#02	Fold#03	Fold#04	Fold#05	Fold#06	Fold#07	Fold#08	Fold#09	Fold#10
2.37%	2.61%	2.90%	3.38%	2.19%	2.42%	2.36%	2.53%	3.28%	2.51%

mode network (DMN) [Raichle et al., 2001; Fox and Raichle, 2007], as highlighted by the yellow circles in Figure 3. The major difference between CFCs #1 and #2 is that there are more connectivities between the anterior and posterior nodes of the DMN in CFC #2. CFCs #3 and #4 involve activities in the DMN, but exhibit more connections between two hemispheres as highlighted by the yellow circles. A clear difference between CFCs #3 and #4 is that CFC #3 exhibit interhemisphere connections at the visual area and supplementary motor area, while CFC #4 shows more interhemisphere connections at the superior part of the central sulcus. CFC #14 also exhibits activities in the DMN, but involves interhemisphere connections in the occipital lobe as highlighted by the oval shape. In comparison, there are many more strong connections between hemispheres in the parietal lobes in CFCs #5, #6, #7 and #9, though the nodes locations are different, as indicated by the dashed oval shapes. Also, the interhemisphere connection patterns in the occipital lobes also differentiate CFCs #5–#7 and #9, as shown by the oval shapes. The CFC #8 only has very sparse strong connection, suggesting that the brain is really in the "resting state" in this CFC state.

CFCs #10 and #13 show some strong connections in the parietal lob and occipital lobe, but not as dense as those in CFCs #5–#7. CFCs #11 and #15 have widespread connections along the dorsal part of the cortex as illustrated by the oval shapes, though the densities and nodes locations are different. Interestingly, the CFCs patterns #12 and #16 involve strong connectivities of the whole brain, as evident by the widespread red edges in Figure 3. The difference between these two CFCs is that functional connections in CFC #16 are more widespread and strong. These two CFCs demonstrated that the brain scanned in R-fMRI could be in very active state. Notably, the clustering of all of the temporally segmented FCs into 16 representative CFCs is optimal based on the BIC criterion and achieves the maximal separation among these 16 patterns according to the FDDL.

Reproducibility Studies

A 10-fold cross-validation of the derived CFC models was performed on the dataset of control subjects, in order to examine the reproducibility of our results in Figures 2 and 3. The same input data used in identifying CFCs in Figures 2 and 3 was divided into 10 equal portions, each consisting of five subjects (except portion #10 consisting of six subjects). There were approximately 80–110 temporal FC segments in each portion. The cross-validation training data was subsequently constructed by sequentially combining nine portions into one matrix, and the remaining portion was used as the testing data:

$$\begin{aligned} &\mathrm{FCS}_{\mathrm{All}} = \{\mathrm{FCS}_{part\ i} | i = 1, 2, \ldots, 10\},\ \mathrm{FCS}_{\mathrm{Test}} = \{\mathrm{FCS}_{\mathrm{part}\ i} | i = k\} \\ &\mathrm{FCS}_{\mathrm{Train}} = \{\mathrm{FCS}_{\mathrm{part}\ i} | i = 1, 2, k-1, k+1, \ldots, 10\} \end{aligned} \tag{10}$$

Afterwards, the Fisher discriminative dictionaries were learned from each of the 10 training datasets, using the same model parameter ($\lambda_1 = 0.01$, $\lambda_2 = 0.05$) as well as mode order (16 classes) as in "Sixteen CFCs Inferred from R-fMRI Data of Healthy Controls" Section. Each dictionary consisted of 16 subdictionaries, corresponding to the 16 CFC classes in the training dataset. Next, the dictionary was applied to both training and testing datasets to perform the sparse coding, resulting in the projected CFC labels for each temporal FC segment. Also, the connectivity patterns of the 16 CFCs were obtained from training datasets.

To assess and present the cross-validation results, three steps were taken. First, the connectivity patterns of the CFCs obtained in each validation experiment are illustrated in Supporting Information Figure S4, and similar patterns can be found across the results. Second, the distributions (histograms) of the CFCs in each of the 10-fold dataset were compared, and the histograms are shown in Supporting Information Figure S5. Also, a table of histogram comparison is provided in Table II. As shown in the figure and the table, the average relative difference of the CFCs distribution from the training and testing datasets is 2.66%. Considering the average standard deviation of the CFCs distributions from training datasets is 6.53%, it is concluded that there is no substantial difference between the CFCs distributions obtained from the training and testing datasets, and the histogram is consistent across training and testing datasets. Third, the model residual of projecting each temporal segment using the CFCs in each validation experiment was obtained and shown in Supporting Information Figure S6 and summarized in Table III. Similar residual levels through the cross-validation studies indicate that the CFC model performance was consistent in different datasets. In addition, within each validation experiment, the residual of testing data is at comparable level with the training data, suggesting the model's capability in explaining new observations from the same population. Considering these results together, the derived CFCs in Figures 2 and 3 are highly reproducible.

TABLE III. List of average relative residuals from the sparse coding of the training and testing datasets

	Fold#01	Fold#02	Fold#03	Fold#04	Fold#05	Fold#06	Fold#07	Fold#08	Fold#09	Fold#10
Train	49%	48%	47%	50%	47%	50%	49%	43%	45%	43%
Test	59%	61%	61%	65%	57%	63%	58%	69%	63%	61%

Temporal Transition Patterns of FCs

In this section, we examine the group-wise temporal transition patterns of CFCs. As shown previously in Figure 1, brain connectivity strength has state transition behaviors. Also, we found a similar pattern in the CFC indices of the projected temporal FC segments (an example is shown in Supporting Information Fig. S7), suggesting that the brain would maintain its FC pattern for certain length of time and then hop to another pattern. Our premise in analyzing the FC transition pattern is that multiple subjects could share the similar transition patterns, and that each subject's brain would possibly hop back and forth among these representative states [Holtzheimer and Mayberg, 2011]. In this sense, the brain activity in each subject can be described as a dynamic random process that transits through a set of successive projected CFC states S_1, S_2, S_3, ..., S_n, similar to a finite-state machine consisting of 16 states. The transition from any states S_i to its next state S_j is quantified by a group-wise probability P_{ij}. Thus, the transition probabilities obtained from the projected state changes of all 51 control subjects were averaged into a 16×16 state transition matrix (shown in Supporting Information Fig. S8). After averaging over the entire population, 26 cells in the state transition matrix are significantly greater than 0 by one-sample t-test under $P = 0.05$, which are mainly the cells with high averaged transition probability, The connectivity map of those cells is presented as a state flow diagram in Figure 4.

An interesting observation that can be made from Figure 4 is that that CFC #01 and CFC #02, which are the most dominant states across all subjects, serve as the hubs of FC transitions during resting state. For instance, more than half of the CFCs are connected to CFC #01 (#2, #3, #4, #5, #6, #9, #10, #11, #13, #14) and #02 (#1, #3, #4, #7, #8, #9, #12, #15). Importantly, these transition patterns are also reproducible in independent groups of subjects. Considering the connectivity patterns of CFC #01 and CFC #02 are mainly composed of ROIs in the default node network (DMN) (highlighted by yellow circles in Fig. 3), it can be postulated that the DMN plays central roles in functional brain transitions and dynamics.

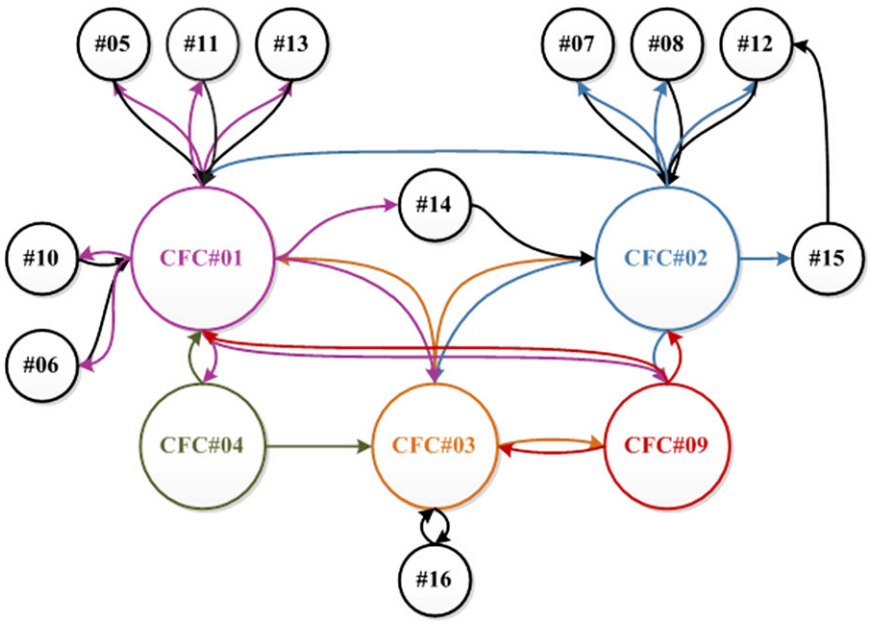

Figure 4.
The state flow diagram depicting significant transitions (transition probability significantly greater than zero at $P = 0.05$; transition from and to CFC state #14, #15, and #16 were also visualized although their probability were not significant) between 16 CFCs in 51 healthy control subjects. Area of the node indicates the total number of temporal FCs segments projected to it.

Altered CFCs and Temporal Dynamics in PTSD

To investigate possible altered CFCs and their abnormal state transition patterns in PTSD, the PTSD patients' R-fMRI datasets were analyzed in the same manner as that in "Temporal Transition Patterns of FCs" Section. In total, 2044 manually segmented FCS_{state} from both healthy control (907 FCS_{state}) and PTSD patients (1137 FCS_{state}) were pooled together. The combined dataset was then equally divided into two groups for training and testing of the CFC models, which forms a 974×358 training matrix A and a 1070×358 testing matrix T. Here, each row in the matrices is the FCS_{state} of manually segmented temporal FC, serving as a training/testing sample. Both the training and testing data contain approximately equal amounts of healthy control and PTSD patient FCS_{state}. We subsequently applied the FDDL method to the training matrix A and learned the corresponding discriminative dictionary. As the training data included both PTSD and control groups, the learned dictionary and corresponding CFCs reflected patterns from both healthy control and PTSD patients. In this study, the BIC was also used for determining the optimal model order (the curve of BIC is shown in Supporting Information Fig. S9). It turned out that for the mixed data, the model with order of 18 (18 CFCs) has the lowest BIC value and is thus selected as the optimal one.

In Figure 5, the connectivity patterns of the 18 CFCs learned from the training matrix A are presented. Interestingly, all of the first 16 CFCs shown in Figure 5 correspond to the 16 CFCs discovered from healthy control subjects shown in Figure 2, indicating the consistency of the CFC models in identifying common connectomes. Strikingly, the last two FC patterns (CFC#17 and CFC#18), also referred to as SFCs, very rarely exist in the learned dictionary obtained from healthy control data at all (occurred in only one out of 51 control subjects), but mostly occur in the PTSD subjects. Furthermore, these two patterns occur widely in the PTSD patients (over 80% of 44 PTSD patients), as seen in the histograms in Supporting Information Figure S10. Considering the fact that all CFCs were learned from the same mixed dataset without a priori knowledge, the clear difference between the CFCs distributions in healthy controls and PTSD patients indicate the high discrimination power of the learned models of CFCs #17 and #18 in separating PTSD patients from controls.

Based on the similar procedures of analyzing the FC dynamics in healthy controls in Figure 4, the state transition probabilities among the 16 normal CFCs and the two PTSD signature SFCs in the mixed dataset were obtained, and the derived state flow diagram is shown in Figure 6. It is apparent that the CFC state transition patterns in PTSD patients are remarkably different from those in the healthy controls, as shown in Figure 4. For instance, CFC #1 becomes the dominant hub of state transitions, while CFC #2 is less active in PTSD patients. This result suggests that the DMN's functional activities are substantially altered in PTSD, in terms of their roles in regulating the functional brain transitions connected to CFCs #1 and #2. Furthermore, the visualizations of the connectivity patterns of the two signature SFCs (CFC#17 and CFC#18) that occur primarily in PTSD patients are provided in the top panels of Figure 6. It is evident that the two abnormal PTSD SFCs are characterized by the hyper-connectivities in the frontal areas and the cingulate gyri, consistent with current neuroscience knowledge about PTSD that has been considered as an anxiety disorder associated with changes in extensive neural circuitries including frontal and limbic systems [Francati et al., 2007]. This result lends support to the validity and effectiveness of our methods and results. The contribution of our work is that we quantitatively modeled and characterized the brain dysfunctions of PTSD via descriptive and rich dynamic functional connectomics signatures.

Two SFCs for the Differentiation of PTSD Patients

The results in the previous sections have shown that CFC #17 and CFC #18 exist dominantly in PTSD patients and that current neuroscience knowledge of PTSD [Francati et al., 2007] lends interpretation of these two SFCs. That is, these two CFCs are characterized by the hyper-connectivities in the frontal areas (e.g., the anterior cingulate cortex (ACC)) and the cingulate gyri, which are believed to be involved in the neural circuitries in PTSD [Francati et al., 2007]. In particular, the hyper-connectivities in the ACC as revealed in the CFC #17 are in agreement with the literature report that enhanced resting metabolic activity in the anterior cingulate cortex (ACC) was associated with PTSD [Shin et al., 2009]. Also, the hyper-connectivities shown in the CFC #18 are consistent with the literature report about the greater increases in blood flow in the posterior cingulate [Bremner et al., 1999]. In this section, we describe the possibility and performance of applying the derived CFC and SFC models to differentiate PTSD patients from healthy controls. Specifically, Figure 7 showed that the two SFCs appear frequently in a majority of PTSD patient subjects. Quantitatively, there were ~80% of 44 PTSD patients with one or more of their FCs throughout the entire time course exhibiting significant project to either or both of these two SFCs. The detailed distributions of two SFCs in 44 PTSD patients are shown in Figure 7. Meanwhile, there was only one healthy control subject out of 51 who exhibited CFC #17. These numbers suggest that the CFC#17 and CFC #18 are intrinsic signature CFC patterns specifically for PTSD patients, and they could be used as potential biomarkers for the individualized differentiation of PTSD patients with quite high sensitivity and specificity.

Studies on the Effect of the Number of DICCCOLs Used for Model Input

In this work, we used the fMRI time series extracted from 358 DICCCOL ROIs as our model input. In order to

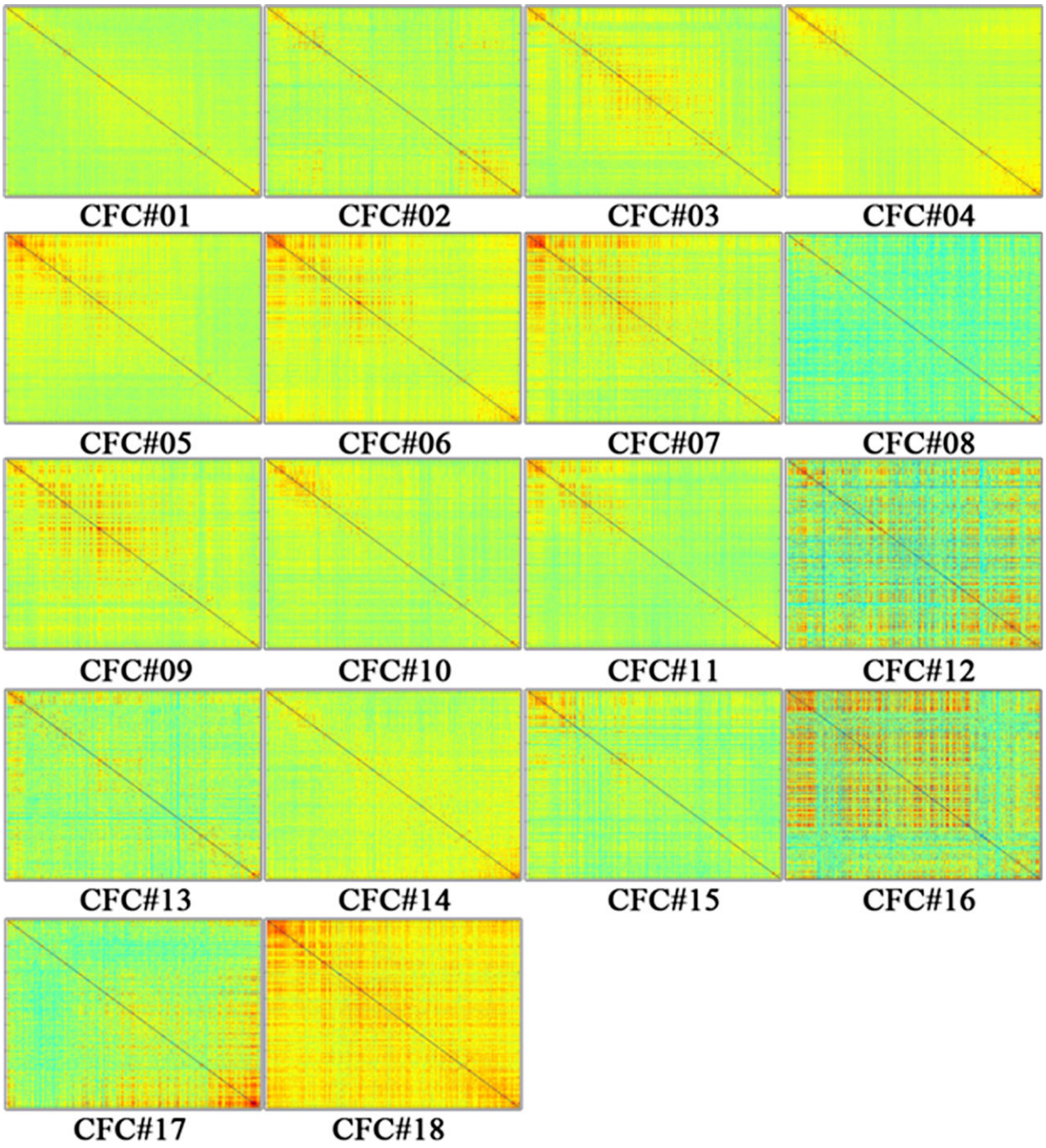

Figure 5.

Visualization of 358 × 358 connectivity patterns of 18 CFCs obtained from mixture of healthy control and PTSD patients. Matrices are color-coded according to the strength of functional interaction from ROI labeled by the column index, to the ROI labeled by the row index. CFCs are ordered to their correspondent CFCs discovered from healthy control subjects in Figure 2, while there are no correspondents of CFC#17 and CFC#18 for healthy controls.

investigate the effect of the relatively high-dimensional input, we also applied our model to learn the dictionary and performed the classification on the data defined on reduced number of ROIs. Three schemes of input ROI reduction were used. In scheme I, we removed certain proportion (10, 25, and 50%) of ROIs which were

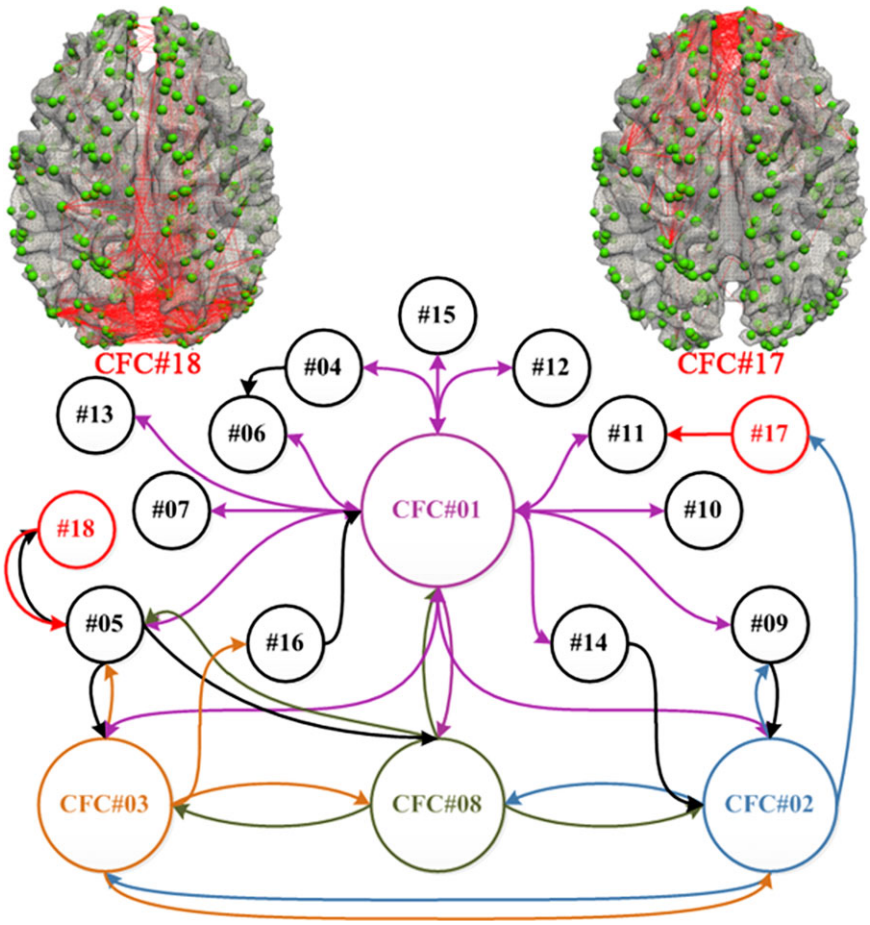

Figure 6.

The state flow diagram depicting significant transitions (transition probability significantly greater than zero at $P = 0.05$; transition from and to states #14, #15, #16, #17, and #18 are also presented although their probabilities were not significant) between CFCs of 44 PTSD patient subjects. Area of the node indicates the total number of temporal FC segments projected to it. Nodes representing state #17 and #18 are colored in red as they are SFCs for PTSD. The patterns of functional connectivities of CFC #17 and #18 on cortical surface are shown to the top panel, where a global threshold (threshold = 0.75 for Pearson's correlation) was used to select the highest functional connectivities shown here. *The state transition matrix of Fig. 6 is shown in Supplemental Figure 11.*

randomly selected from the whole 358 ROIs, keeping a randomly partially covered ROI definition of the brain. In scheme II, we removed the same proportions (10, 25, and 50%) of ROIs with the lowest summed FCS, which indicates their functional connectivity strength through the whole time series, thus keeping those ROIs with stronger functional connection. In scheme III, ROIs were hierarchically clustered by their FCS vectors, where the same proportions (10, 25, and 50%) of "outlier" ROIs (i.e., those with FCS vector distant apart from other ROIs) were removed. After the reduction of ROIs, the model was trained and tested using the similar method as in previous health control/PTSD classification described in "Altered CFCs and Temporal Dynamics in PTSD and Two SFCs for the Differentiation of PTSD Patients" Sections. We obtained the two CFCs that had the highest proportion in PTSD data to serve as the SFC for PTSD patient classification with reduced ROIs, listed in the "proportion" columns in Table IV. It is noted that in the result of the model using the original 358 DICCCOL ROIs, the proportion of CFC#17 and CFC#18 in PTSD dataset were 98 and 100%. The experiment here shows that reducing the number of ROIs by less than 10% would not affect the model performance much, while the model results would be infeasible when more than half of the ROIs were removed, where there was only one SFC identified in scheme II with significantly high proportion in PTSD data, and no SFCs identified in scheme I and III. We also compared the

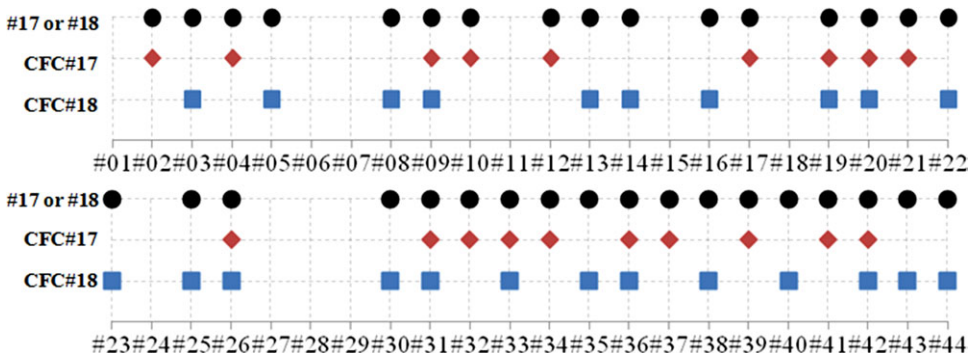

Figure 7.

The SFC distributions in 44 PTSD patients. Indices at *y*-axis are PTSD subjects. The mark on each subject indicates that this subject had one or more of its temporal FCs segments projected to the corresponding SFCs (CFC#17 and/or CFC18). The union of them ("#17 or #18" of black mark) serves as the criteria for identifying a specific subject as PTSD patient.

functional connectivity pattern of the two SFCs from reduced data with the SFCs obtained from the original data. The similarities were only calculated on the ROIs defined in both settings, and the values are listed in the "similarity" columns in the table. Generally with less than 25% ROIs removed the result is still reasonably good, only with minor alterations of the two SFCs, especially on data that are more homogeneous (scheme III). Although on data with 50% ROIs removed, there would be substantial loss of coverage of the brain functions, thus reducing the feasibility of the model.

Studies on the Effect of Model Order Selection

To investigate the model sensitivity to the number of classes used during the optimization and classification, we tested our model by using various numbers of classes on the mixed (healthy control and PTSD patients) data as described in "Altered CFCs and Temporal Dynamics in PTSD" Section. For each experiment (e.g., running the model on 17, rather than 18 classes), we obtained the CFCs using the same method and model parameters as in "Altered CFCs and Temporal Dynamics in PTSD" Section. We then compared their corresponding functional connectivity patterns with the 18 CFCs obtained in "Altered CFCs and Temporal Dynamics in PTSD," which is regarded as the basic patterns in this experiment. By the comparison we could find the matching of CFCs between the model results using different model orders. For example, by using model order of 17 (i.e., 17 classes) in running the model, we observed that the least matching CFC in basic patterns with those 17 CFCs from the model results is CFC#16, indicating that this CFC was "merged" into other classes when the number of classes was reduced. Similarly, by increasing the model order and conduct the comparison between the obtained CFC and basic patterns, we found that the additional CFCs would be "split" from the 18 basic patterns. The detailed changing of CFCs with the different number of classes is listed in the Table V below. The table shows that only when the model order is reduced to 11, the SFCs used for classification (CFC#18 or CFC#17) would be merged to other CFCs, that renders the model unable to classify the patients with normal controls.

TABLE IV. Result of the model classification accuracy and the similarities of the SFCs for classification obtained from data defined on reduced numbers of ROIs

# of ROIs	Scheme	Similarity of CFC#17	Similarity of CFC#18	Proportion of CFC#17inPTSD	Proportion of CFC#18inPTSD
322	I	82%	80%	85%	84%
268	I	78%	65%	71%	73%
179	I	N/A	N/A	N/A	N/A
322	II	79%	85%	87%	91%
268	II	66%	70%	80%	73%
179	II	69%	N/A	72%	N/A
322	III	92%	95%	92%	95%
268	III	83%	78%	82%	88%
179	III	N/A	N/A	N/A	N/A

TABLE V. The relationship between the changing of CFCs and the model order (number of classes)

11 classes	12 classes	13 classes	14 classes	15 classes	16 classes	17 classes	18 classes	19 classes	20 classes	21 classes	22 classes
Remove CFC#18	Remove CFC#12	Remove CFC#17	Remove CFC#11	Remove CFC#9	Remove CFC#6	Remove CFC#16	N/A	CFC#10 Split	CFC#13 Split	CFC#7 Split	CFC#21 Split

The CFCs obtained by using model order of 18 is regarded as basic, and all the other result were derived from the comparison with the basic patterns.

Conversely, when the model order was increased to as large as 22, the two SFCs was still intact and the model retains its classification capacity.

Model Parameter Estimation by Stability Selection Method

In addition to the method used in "CFC Modeling" Section for the estimation of model parameters λ_1 and λ_2, which aims at optimizing the model capacity of classifying normal controls/patient subjects, we have used the stability selection method [Meinshausen, 2010] to obtain the stable FCS_{state} involved in the dictionary learning process of FDDL modeling. In this work, we used the stability selection method by first selecting a model parameter λ_1. Then we used the bootstrapping methodology to perform N times of random resampling of the control training dataset containing 907 number of FCS_{state}, and obtained N (set to 1,000 in this study) number of new datasets, which were of the same size as the original dataset but may contain duplicate values as the sampling is with replacement. The FDDL dictionary learning was thus applied on the new datasets with the predetermined parameter λ_1. Then the probability of a specific item $FCS_{state\text{-}i}$ being included in the subdictionary D_m could be obtained by the following equation [Ye, et al., 2012]:

$$P_i^m = \sum \mathrm{If}(X_i^m > 0)/N \tag{11}$$

where If(·) is the indicator function of whether the specific item is included in the corresponding subdictionary. For each model parameter λ_1 used in the above analysis, we could obtain one corresponding P_i^m that measures the probability of the ith FCS_{state} used in the mth subdictionary. In this work, we have tried 11 values of λ_1 ranging from 0 to 1 by a step of 0.05. Thus for each FCS_{state}, there would be 21 probability vectors corresponding to each model parameter. Then, the set of stable FCS_{state} is defined by congregating all FCS_{state} whose maximum probability over all of the 21 parameters in all of m subdictionaries exceeding a predefined threshold τ (set to 0.7 in this study). For instance, if a specific FCS_{state} has at least one frequent (thresholded by τ) occurrence in any of the subdictionaries in any parameter used, it would be considered as stable. The experiment results are shown in the Table VI. It can be seen from Table VI that there is at least one stable FCS_{state} corresponding to each of the 16 subdictionaries learned, suggesting the good capability of the proposed methods in analyzing the FC dynamics. The functional connectivity maps of the brain states which the stable FCS_{state} belong to are visualized in Supporting Information Figure S12.

DISCUSSION AND CONCLUSION

In this study, we applied the Fisher discrimination dictionary learning sparse coding approaches to identify CFCs from temporally divided quasi-static FC segments obtained from resting state fMRI data. Both structural and FCs were derived via our recently established 358 DICCCOL ROIs [Zhu et al. 2012b]. The optimal number of CFCs was determined by the minimization of Bayesian information criterion. In the 16 reproducible CFCs in healthy control brains identified in independent datasets by our methods, there existed two CFCs (CFC #1 and CFC #2) that are mainly composed of the DMN [Raichle et al., 2001; Damoiseaux et al., 2006; Fox and Raichle, 2007] ROIs, and they occur frequently throughout the entire scan time course and serve as the hubs for temporal CFC transitions. This novel finding suggests the important roles of DMN in functional brain state transitions and dynamics.

Furthermore, by analyzing the mixed data of healthy controls and PTSD patients together, we found that healthy controls and PTSD patients shared a large number of common connectome patterns, as the 16 CFCs derived

TABLE VI. The stability selection result on healthy control training dataset

FCS state	7	39	203	236	237	282	304	378	412	464	474	503	541	584	624	682	693	891
Frequency	89%	84%	81%	84%	75%	79%	76%	83%	81%	83%	83%	82%	82%	84%	81%	84%	83%	78%
Class	6	1	7	13	15	14	14	3	11	2	9	16	8	15	4	10	5	12

The first row is the indices of the training samples (from 1 to 907). The second row is the maximum frequency of the sample being included in a specific subdictionary. The third row is the indices of the class (subdictionary) most frequently using that sample.

from healthy control subjects were all present in PTSD patients. This result not only demonstrates the commonality of FCs in healthy controls and PTSD patients, but also reveals the reproducibility of the CFCs in different populations. Furthermore, we identified two additional CFCs that existed primarily in PTSD patient subjects, which were then defined as PTSD SFCs. Further examination of these two SFCs revealed abnormal hyper-connectivities in the frontal cortex and cingulate gyri of the PTSD patients, consistent with current neuroscience knowledge about PTSD [Bremner and Charney, 1994; Francati et al., 2007]. Interestingly, these two SFCs occur frequently in PTSD subjects but very rarely in healthy controls, and they alone can differentiate 80% of individual PTSD subjects from healthy controls with very low false positive of 2%.

Additionally, the temporal transition patterns among those CFCs in both healthy control and PTSD patient subjects were analyzed, and substantial and meaningful differences between their transition patterns were discovered, in agreement with the concept of brain states modeling for psychiatric conditions in psychiatry literatures. For instance, in 2011, Holtzheimer and Mayberg postulated that in major depressive disorder could be defined as the tendency to enter into, and inability to disengage from, a negative mood state rather than the mood state per se. Though the CFCs and FSM modeling in our work for PTSD patients would not necessarily correspond to the state models in the depression study, the present work shares the similar concepts of abstracting brain functional activity as brain states and representing mental status by a finite state transition space. In particular, our work has demonstrated the existence of abnormal functional SFCs that are specific for PTSD patients, providing direct support to the concept of diseased functional brain states in psychiatric conditions [Holtzheimer and Mayberg, 2011].

The work presented in this article can be further enhanced in the following directions. First, as noted by several researchers [Goebel et al., 2003; Stephan et al., 2009] and other reports, structural brain connectivity could be helpful in guiding the modeling of functional brain connectivity. Hence, we plan to develop new models to analyze FC dynamics based on both functional and structural connectivity of DICCCOL ROIs in the future. The joint modeling of multimodal neuroimaging data would potentially improve the model stability both within (e.g., through different scan sessions) and across subjects. Also, by adding structural information, we could better interpret the model result (CFCs and state transition) with more anatomical and neuroscience implication. Second, we plan to employ more sophisticated modeling methods to describe the FC transition patterns. As shown in the state flow diagram of healthy control and PTSD patient subjects, the transition pattern modeling is a powerful tool in analyzing, combining and comparing brain dynamics across subjects and populations. Currently, only the adjacent state change is considered in this work, which is the simplest feature of random processes (e.g., first-order Markov chain). We already observed that there exist high-order dependencies between states, that is, not only the current state determines how the brain transit to the next state but also the previous states would affect the transition. By utilizing higher-order random process analysis in the future, we would be able to model such characteristics of higher-order brain state transitions, providing a new way of understanding how the brain functions dynamically.

Structural and functional connectivity analysis via multimodal DTI/R-fMRI data has offered exciting opportunities to understand the functions and dysfunctions in healthy brains and a variety of neurological/psychiatric diseases [Rogers et al., 2007; Zang et al., 2007; Castellanos et al., 2008; Buckner et al., 2009; Church et al., 2009; Rombouts et al., 2009; Li et al., in press], including schizophrenia [Whalley et al., 2005; Liang et al., 2006] and Alzheimer's disease [Li et al., 2002, Wang et al., 2006]. The dynamic functional connectomics mapping methods in this article have revealed PTSD SFCs and their temporal transition patterns that can effectively characterize and differentiate PTSD subjects from healthy controls. We envision that this school of dynamic functional connectomics mapping methodologies can be potentially applied to reveal intrinsic pathological brain activities in many other brain conditions and contribute to the development and validation of effective biomarkers of those brain illnesses in the future.

REFERENCES

Black PE (2008): Finite State Machine. In: Black PE, editor. Dictionary of Algorithms and Data Structures

Bremner JD, Charney DS. (1994): Neurobiology of posttraumatic stress disorder: Implications for treatment. In: Darcourt G, Mendlewicz J, Racagni G, Brunello N, editors. Current therapeutic approaches to panic and other anxiety disorders. Int Acad Biomed Drug Res. 8:171–186.

Bremner JD, Narayan M, Staib LH, Southwick SM, McGlashan T, Charney DS (1999): Neural correlates of memories of childhood sexual abuse in women with and without posttraumatic stress disorder. Am J Psychiatry 156:1787–1795.

Buckner RL, Sepulcre J, Talukdar T, Krienen FM, Liu H, Hedden T, Andrews-Hanna JR, Sperling RA, Johnson KA (2009): Cortical Hubs Revealed by Intrinsic Functional Connectivity: Mapping, Assessment of Stability, and Relation to Alzheimer's Disease. J Neurosci 29:1860–1873.

Castellanos FX, Margulies DS, Kelly C, Uddin LQ, Ghaffari M, Kirsch A, Shaw D, Shehzad Z, Di Martino A, Biswal B, Sonuga-Barke EJS, Rotrosen J, Adler LA, Milham MP (2008): Cingulate-Precuneus Interactions: A New Locus of Dysfunction in Adult Attention-Deficit/Hyperactivity Disorder. Biol Psychiatry 63:332–337.

Chang C, Glover GH (2010): Time-frequency dynamics of resting-state brain connectivity measured with fMRI. NeuroImage 50: 81–98.

Church JA, Fair DA, Dosenbach NUF, Cohen AL, Miezin FM, Petersen SE, Schlaggar BL (2009): Control networks in paediatric Tourette syndrome show immature and anomalous patterns of functional connectivity. Brain 132:225–238.

Damoiseaux JS, Rombouts SARB, Barkhof F, Scheltens P, Stam CJ, Smith SM, Beckmann CF (2006): Consistent resting-state networks across healthy subjects. Proc Natl Acad Sci USA 103:13848–13853.

Derrfuss J, Mar RA (2009): Lost in localization: The need for a universal coordinate database, NeuroImage 48:1–7.

Dickerson BC, Sperling RA (2009): Large-scale functional brain network abnormalities in Alzheimer's disease: Insights from functional neuroimaging, Behav Neurol 21:63–75.

Duda RO, Hart PE, Stork DG (2000): Pattern Classification. 2nd ed. New York, NY: Wiley-Interscience.

Fonzo GA, Simmons AN, Thorp SR, Norman SB, Paulus MP, Stein MB (2010): Exaggerated and disconnected insular-amygdalar blood oxygenation level-dependent response to threat-related emotional faces in women with intimatepartner violence posttraumatic stress disorder. Biol Psychiatry 68:433–441.

Fox M, Raichle M (2007). Spontaneous fluctuations in brain activity observed with functional magnetic resonance imaging. Nat Rev Neurosci 8:700–711.

Francati V, Vermetten E, Bremner JD (2007): Functional neuroimaging studies in posttraumatic stress disorder: review of current methods and findings. Depress Anxiety 24:202–218.

Gilbert CD, Sigman M (2007): Brain states: Top-down influences in sensory processing. Neuron 54:677–696.

Goebel R, Roebroeck A, Kim D-S, Formisano E (2003): Investigating directed cortical interactions in time-resolved fMRI data using vector autoregressive modeling and Granger causality mapping. Magn Reson Imaging 21:1251–1261.

Hagmann P, Cammoun L, Gigandet X, Gerhard S, Grant PE, Wedeen V, Meuli R, Thiran JP, Honey, CJ, Sporns O (2010): MR connectomics: Principles and challenges. J Neurosci Methods 194:34–45.

Holtzheimer PE, Mayberg HS (2011): Stuck in a rut: rethinking depression and its treatment. Trends in Neurosciences 34:1–9.

Hughes K, Shin L (2011): Functional neuroimaging studies of post-traumatic stress disorder. Expert Rev Neurother 11: 275–285.

Kennedy DN (2010): Making connections in the connectome era. Neuroinformatics 8:61–62.

Koenig T, Lehmann D, Merlo MCG, Kochi K, Hell D, Koukkou M (1999): A deviant EEG brain microstate in acute, neuroleptic-naive schizophrenics at rest. Eur Arch Psychiatry Clin Neurosci 249:205–211.

Koenig T, Prichep L, Lehmann D, Sosa PV, Braeker E, Kleinlogel H, Isenhart R, John ER (2002): Millisecond by millisecond, year by year: Normative EEG microstates and developmental stages. NeuroImage 16:41–48.

Lanius RA, Bluhm RL, Coupland NJ, Hegadoren KM, Rowe B, Théberge J, Neufeld RWJ, Williamson PC, Brimson M (2010): Default mode network connectivity as a predictor of post-traumatic stress disorder symptom severity in acutely traumatized subjects. Acta Psychiatr Scand 121:33–40.

Lehmann D, Michel CM, Pal I, Pascual-marqui RD (1994): Event-related potential maps depend on prestimulus brain electric microstate map. Int J Neurosci 74:239–248.

Lehmann D, Strik WK, Henggeler B, Koenig T, Koukkou M (1998): Brain electric microstates and momentary conscious mind states as building blocks of spontaneous thinking. I. Visual imagery and abstract thoughts. Int J Psychophysiol 29:1–11.

Li S-J, Li Z, Wu G, Zhang M-J, Franczak M, Antuono PG (2002): Alzheimer disease: Evaluation of a functional MR imaging index as a marker. Radiology 225:253–259.

Li K, Guo L, Faraco C, Zhu D, Deng D, Zhang T, Jiang X, Zhang D, Chen H, Hu HL, Miller S, Liu T (2010) Individualized ROI Optimization via Maximization of Group-wise Consistency of Structural and Functional Profiles. Adv Neural Info Proc Syst 23:1369–1377.

Li K, Zhu D, Guo L, Li Z, Lynch ME, Coles C, Hu X, Liu T: Connectomics signatures of prenatal cocaine exposure affected adolescent brains. Human Brain Mapp (in press).

Li X, Lim C, Li K, Guo L, Liu T: Detecting brain state changes via fiber-centered functional connectivity analysis. Neuroinformatics 1–18.

Liang M, Zhou Y, Jiang T, Liu Z, Tian L, Liu H, Hao Y (2006): Widespread functional disconnectivity in schizophrenia with resting-state functional magnetic resonance imaging. Neuroreport 17:209–213.

Liu T (2011): A few thoughts on brain ROIs. Brain Imaging Behav 5:189–202.

Lynall ME, Bassett DS, Kerwin R, McKenna PJ, Kitzbichler M, Muller U, Bullmore E (2010): Functional connectivity and brain networks in schizophrenia. J Neurosci 30:9477–9487.

Majeed W, Magnuson M, Hasenkamp W, Schwarb H, Schumacher EH, Barsalou L, Keilholz SD (2011): Spatiotemporal dynamics of low frequency BOLD fluctuations in rats and humans. Neuroimage 54:1140–1150.

Meinshausen N, Bühlmann P (2010): Stability selection (with discussion). J R Stat Soc B 72:417–473.

Meng Y, Zhang D, Xiangchu F, Zhang D (2011): Fisher discrimination dictionary learning for sparse representation. In: Computer Vision and Pattern Recognition (CVPR), 2011 IEEE Conference on , pp 543–550.

Niedermeyer E, Silva FLD (2004): Electroencephalography: Basic Principles, Clinical Applications, and Related Fields. Electroencephalography: Basic Principles, Clinical Applications, and Related Fields. Philadelphia, PA: Lippincott Williams & Wilkins.

Olshausen BA, Field DJ (1996). Emergence of simple-cell receptive field properties by learning a sparse code for natural images. Nature 381:607–609.

Pascual-Marqui RD, Michel CM, Lehmann D (1995): Segmentation of brain electrical activity into microstates: model estimation and validation. IEEE Trans Biomed Eng 42:658–665.

Passingham RE, Stephan KE, Kotter R (2002): The anatomical basis of functional localization in the cortex. Nat Rev Neurosci 3: 606–616.

Poldrack RA (in press): The future of fMRI in cognitive neuroscience, Neuroimage 62:1216–1220.

Qiang Z, Baoxin L (2010): Discriminative K-SVD for dictionary learning in face recognition. In: Computer Vision and Pattern Recognition (CVPR), 2011 IEEE Conference on , pp 2691–2698.

Raichle ME, MacLeod AM, Snyder AZ, Powers WJ, Gusnard DA, Shulman GL (2001): A default mode of brain function. Proc Natl Acad Sci USA 98:676–682.

Ramirez I, Sprechmann P, Sapiro G (2010): Classification and clustering via dictionary learning with structured incoherence and shared features, In: Computer Vision and Pattern Recognition (CVPR), 2010 IEEE Conference on, pp 3501–3508.

Rogers BP, Morgan VL, Newton AT, Gore JC (2007): Assessing functional connectivity in the human brain by fMRI. Magn Reson Imaging 25:1347–1357.

Rombouts SARB, Damoiseaux JS, Goekoop R, Barkhof F, Scheltens P, Smith SM, Beckmann CF (2009): Model-free group analysis shows altered BOLD FMRI networks in dementia. Hum Brain Mapp 30:256–266.

Schwarz G (1978): Estimating the dimension of a model. Ann Stat 6:461–464.

Shin LM, Lasko NB, Macklin ML, Karpf RD, Milad MR, Orr SP, Goetz JM, Fischman AJ, Rauch SL, Pitman RK (2009): Resting metabolic activity in the cingulate cortex and vulnerability to posttraumatic stress disorder. Arch Gen Psychiatry 66: 1099–1107.

Smith SM, Miller KL, Moeller S, Xu J, Auerbach EJ, Woolrich MW, Beckmann CF, Jenkinson M, Andersson J, Glasser MF, Van Essen DC, Feinberg DA, Yacoub ES, Ugurbil K (2012): Temporally-independent functional modes of spontaneous brain activity. Proc Natl Acad Sci USA 109:3131–3136.

Sporns O, Tononi G, Kötter R (2005): The human connectome: A structural description of the human brain. PLoS Comput Biol 1:e42.

Stephan KE, Tittgemeyer M, Knösche T, Moran R, Friston K (2009): Tractography-based priors for dynamic causal models. Neuroimage 47:1628–1638.

Van KR, Hedden T, Venkataraman A, Evans KC, Lazar SW, Buckner RL (2010): Intrinsic functional connectivity as a tool for human connectomics: Theory, properties, and optimization. J Neurophysiol 103:297–321.

Wang L, Zang Y, He Y, Liang M, Zhang X, Tian L, Wu T, Jiang T, Li K (2006): Changes in hippocampal connectivity in the early stages of Alzheimer's disease: Evidence from resting state fMRI. Neuroimage 31:496–504.

Whalley HC, Simonotto E, Marshall I, Owens DGC, Goddard NH, Johnstone EC, Lawrie SM (2005): Functional disconnectivity in subjects at high genetic risk of schizophrenia. Brain 128: 2097–2108.

Williams R (2010): The human connectome: just another 'ome? Lancet Neurol. 9:238–239.

Wright J, Yang AY, Ganesh A, Sastry SS, Ma Y (2009): Robust face recognition via sparse representation. IEEE Trans Pattern Anal Mach Intell 31:210–227.

Ye J, Farnum M, Yang E, Verbeeck R, Lobanov V, Raghavan N, Novak G, DiBernardo A, Narayan VA (2012): Alzheimer's disease neuroimaging initiative, sparse learning and stability selection for predicting MCI to AD conversion using baseline ADNI data. BMC Neurol 12:46; doi:10.1186/1471–2377-12–46.

Yu-Feng Z, Yong H, Chao-Zhe Z, Qing-Jiu C, Man-Qiu S, Meng L, Li-Xia T, Tian-Zi J, Yu-Feng W (2007): Altered baseline brain activity in children with ADHD revealed by resting-state functional MRI. Brain Dev 29:83–91.

Zhang T, Guo L, Li K, Jing C, Yin Y, Zhu D, Cui G, Li L, Liu T (2012): Predicting functional cortical ROIs via DTI-derived fiber shape models. Cereb Cortex 22:854–864.

Zhang X, Guo L, Li X, Zhu D, Li K, Sun Z, Jin C, Hu X, Han J, Zhao Q, Li L, Liu T (2012): Characterization of Task-free/Task-performance Brain States. In: Ayache N, Delingette H, Golland P, Mori K, editors. Medical Image Computing and Computer-Assisted Intervention – MICCAI 2012. Berlin, Heidelberg: Springer. p 237–245.

Zhu D, Zhang D, Faraco C, Li K, Deng F, Chen H, Jiang X, Guo L, Miller LS, Liu T (2011b): Discovering dense and consistent landmarks in the brain. In: Proceedings of the 22nd international conference on Information processing in medical imaging. Kloster Irsee, Germany: Springer-Verlag. p. 97–110.

Zhu D, Li K, Faraco CC, Deng F, Zhang D, Guo L, Miller LS, Liu T (2012a): Optimization of functional brain ROIs via maximization of consistency of structural connectivity profiles. Neuroimage 59:1382–1393.

Zhu D, Li K, Guo L, Jiang X, Zhang T, Zhang D, Chen H, Deng F, Faraco C, Jin C, Wee C, Yuan Y, Lv P, Yin Y, Hu X, Duan L, Hu X, Han J, Wang L, Shen D, Miller L S, Li L, Liu T (2012b): DICCCOL: Dense individualized and common connectivity-based cortical landmarks. Cereb Cortex.

Zilles K, Amunts K (2010): Centenary of Brodmann's map—Conception and fate. Nat Rev Neurosci 11:139–145.